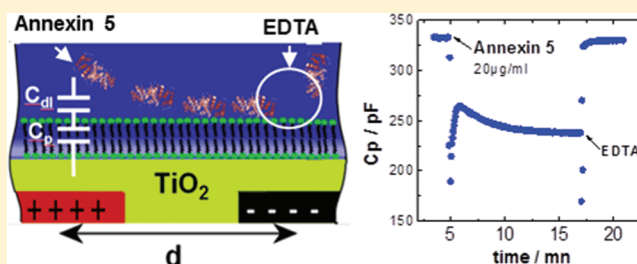Article

# Characterization of Double Layer Alterations Induced by Charged Particles and Protein−Membrane Interactions Using Contactless Impedance Spectroscopy

Jan Steinkuehler, Verena Charwat, Lukas Richter, and Peter Ertl*

AIT Austrian Institute of Technology GmbH, Muthgasse 11/2, 1190 Vienna, Austria

**ABSTRACT:** Double layer interactions between charged particles and surfaces play a vital role in a variety of technical and biological systems because they determine the stability of, e.g., protein−membrane biointerfaces. The underlying theoretical principle is based on the overlap of two different double layers that induce surface charges to be shifted to a new equilibrium distribution, which can be approximated by the Poisson−Boltzmann equation. In the present work we show theoretical and experimental results involving double layer capacitance of surfaces that exhibit charge regulation behavior.



Charge regulation is an important parameter to consider when investigating protein−membrane interactions because it defines surface properties between ideal constant charge and constant potential behavior. In this work we introduce a novel theoretical model that also includes charge regulation behavior and can assess changes of double layer disruptions at $TiO_2$ and supported lipid-bilayers (SLB). The selected surfaces represent important biointerfaces that can be found on implants or cell membranes. We also demonstrate that contactless impedance spectroscopy is well suited to measure double layer capacitance interactions using differently charged silica beads. The combination of a theoretical model with experimental data allowed us further to identify charge regulation effects during protein adsorption (BSA and Annexin V) events at supported lipid-bilayers (SLB) used as a simple cell membrane model. Finally, the first indications of changed charge regulation behavior during protein surface crystallization events were also documented.

## INTRODUCTION

Double layer interactions play a key role in colloid science, including biological and technical systems, because they influence the stability of colloids, including particle−surface interfaces.[1,2] In liquid solutions a charged particle is surrounded by a diffusive ionic layer that screens the electrical potential at the surface. The diffuse part of the electrical potential in close proximity of a charged surface can be described by the Poisson−Boltzmann (PB) equation, which is a mean field approximation that is still widely used despite several shortcomings including the disregard of ion size and hydration effects.[3] The calculated charge distribution due to the double layer interaction depends on the electrolyte concentration and boundary conditions at the surfaces.[4] Two common boundary conditions are employed in the PB calculation: constant potential (CP) and constant charge (CC). Under real conditions charged surfaces do not exhibit either CP or CC, and therefore, a charge regulating boundary (CR) needs to be considered. This is based on the fact that the surface charge depends on the local pH (local potential) due to association or dissociations of the potential determination ions.[5−7] The CR boundary condition employed in this work can be used to estimate values on resulting double layer interactions between CP and CC using an approximation of CR behavior that includes CR effects into a single parameter.[6,7] AFM is the method commonly used to estimate CR effects and to determine double layer interactions between a charged particle and a surface; AFM force measurements provide information on electrostatic repulsions or attractions. It is well established that, under a wide range of experimental conditions, PB theory can account for measured forces, even if deviations are frequently observed.[8−10] Although successfully used to estimate surface forces and double layer interactions of charged particles, force measurements based on AFM are not suitable for a wide range of biological applications where global signals and noninvasive measurement conditions are required.

In turn, impedance spectroscopy is suitable to address double layer interactions of charged particles at biointerfaces based on the assessment of changes at the double layer capacitance. In addition to miniaturization and automation capabilities, the main advantage of employing impedance spectroscopy is its compatibility with biological in vitro systems. Several studies have successfully demonstrated that impedance spectroscopy can be used to measure changes in the double layer capacitance following adsorption of a biological species such as DNA or proteins.[11−14] Additionally, a modified PB equation that also

includes charge regulation properties of adsorbed species has also been employed to accurately estimate the amount of lysozyme adsorbed onto a surface.[15,16] A similar model was also recently used to calculate the double layer capacitance changes upon adsorption of proteins at an oil−water interface.[14]

In the current work, new theoretical and experimental approaches are used to estimate double layer capacitance changes at the biointerface. In the new theoretical model, both the surface and the adsorbed particle as a boundary for the PB equation are considered. The theoretical model consists of the relation between (linear) double layer capacitance and the varying boundary conditions of both the surface and the adsorbed particle. The experimental part of the study consists of using contactless impedance spectroscopy to detect capacitance changes in the presence of charged particles and proteins. Interdigitated electrode structures ($\mu$IDES) covered by a uniform 120 nm thick $TiO_2$ layer for contactless dielectric sensing were used. Dielectric sensing is a label-free and noninvasive method traditionally used to measure polarization responses of low dielectric materials such as (bio)polymers, proteins, or cells exposed to radio frequency electrical fields.[17] We have recently reported the integration of high-density microinterdigitated electrodes in various biochips for the noninvasive monitoring of microbial biofilms, virus contamination, liposomes and mammalian cells.[18] In a previous work we have also demonstrated that contactless impedance measurements provide stable and nondrifting signals over long periods of time due to complete sensor insulation and physical removal from the liquid sensing environment.[19] In that contactless configuration the analyte under investigation is not influenced by electrochemical reactions that may take place at a conducting electrode surface.[20] The absence of faradaic currents or pseudocapacitive influence of redox reactions, even by low concentrated impurities in the analyte, is of particular importance because they could interfere with the monitoring of double layer capacitance changes.[21] Contactless impedance microsensors are therefore ideally suited for detecting double layer disruptions induced by charged particles and protein−membrane interactions. In the current work contactless impedance spectroscopy is applied to investigate double layer disruptions at important biointerfaces such as $TiO_2$ surfaces, which are commonly found in implants, and lipid-bilayers, which are a major cell membrane component. Initially, double layer disruptions in the presence of silica and amino-terminated silica beads exhibiting various surface charges are used to validate the theoretical model. The new model is applied to monitor protein adsorptions kinetics of two different proteins (BSA and Annexin V) at supported lipid-bilayers.

## ■ METHODS AND MATERIALS

**Theoretical Methods.** For simplicity two, planar and indefinitely extended, charged surfaces separated in a monovalent electrolyte by a distance $2L$ are assumed. According to Stern theory, charges from the electrolyte bind to the surface and are immobilized. These charges are then screened by a diffuse layer of ions. The PB equation for the potential can be written as[22]

$$\nabla^2 \psi = \frac{2c_0 e}{\varepsilon \varepsilon_0} \sinh\left(\frac{e\psi}{k_B T}\right) \qquad (1)$$

where $\psi$ represents the diffuse layer potential, $e$ is the magnitude of the electronic charge, $k_B$ is the Bolzman

constant, and $T$ the absolute temperature. The parameter $\kappa$ is called the inverse Debay length $\kappa = ((2c_0 e^2)/(\varepsilon \varepsilon_0 k_B T))^{1/2}$, with $c_0$ the ion concentration in number/L. The linearized form of eq 1 is called the Debye−Hückel approximation (DH) and is valid for small potentials only.[4]

$$\nabla^2 \Psi = \kappa^2 \Psi \qquad (2)$$

For a 1D-system the general solution to (2) is

$$\Psi(x) = A \exp(\kappa x) + B \exp(-\kappa x) \qquad (3)$$

where $A$ and $B$ represent real numbers. The solutions of (1) and (2) are obtained by solving for different boundary conditions and separations $d$. A one-dimensional system is considered with boundaries at $x_0 = -d$, $x_1 = +d$, the distance between the two surfaces is then $L = 2d$. Two possible boundary conditions are constant potential (CP) or constant charge (CC)

$$\psi(x_{0,1}) = \psi_0$$

$$\pm \frac{d\psi}{dx}\bigg|_{x=x_{0,1}} = \frac{-\sigma_0}{\varepsilon \varepsilon_r} \qquad (4)$$

where $\Psi_0, \sigma_0$ are the scaled potential or charge. Analog boundary conditions are set for $x_2$. Real surfaces usually show a behavior between CC and CP. For a wide range of surfaces this behavior can be approximated linearly by introducing a so-called regulation capacitance ($C_I$).[23,6] The boundary can then be written as (for the nonscaled potential)

$$\varepsilon \varepsilon_0 \pm \frac{d\psi}{dx}\bigg|_{x=x_0} = \sigma_{L \to \infty} - C_I(\psi - \psi_{L \to \infty}) \qquad (5)$$

where $C_I = -\partial \sigma_{L \to \infty}/\partial \psi$ and $\sigma_{L \to \infty}$ refers to the surface charge at infinite separation of the surfaces. The charge regulation capacitance can be found by determining the slope in, e.g., experimental titration curves. The model can be further simplified by introducing a regulation parameter defined as[6]

$$p = \frac{C_D}{C_I + C_D} \qquad (6)$$

The parameter $p$, usually between 0 and 1, defines if a surface shows a rather a CP ($p \to 0$) or CC ($p \to 1$) type behavior. The charge regulation boundary can also be determined by introducing a model for the surface charges, e.g., the 1-p$K$ model and solving the full nonlinear system of the PB and the surface charge equations. However, using a dimensionless parameter has the advantage that it does not depend on a model that is unavailable for complex systems. The parameter $p$ can be obtained experimentally for an isolated surface and was found to describe double layer interaction even for small separation.[6] Additionally, a regulation capacitance was also proposed for protein−protein and protein−membrane interaction out of statistical mechanical approach.[24] This further supports the use of this approximation. For $0 < p < 1$ the interaction energy, and hence also the force, lies between the two solutions found for CP and CC boundaries. That is why CP and CC are frequently used as an upper or lower bound for the double layer interaction.[6] For CP or CC boundaries parameters $A$ and $B$ from eq 3 can be easily found. The differential double layer capacitance of the diffusive part is then found by calculating
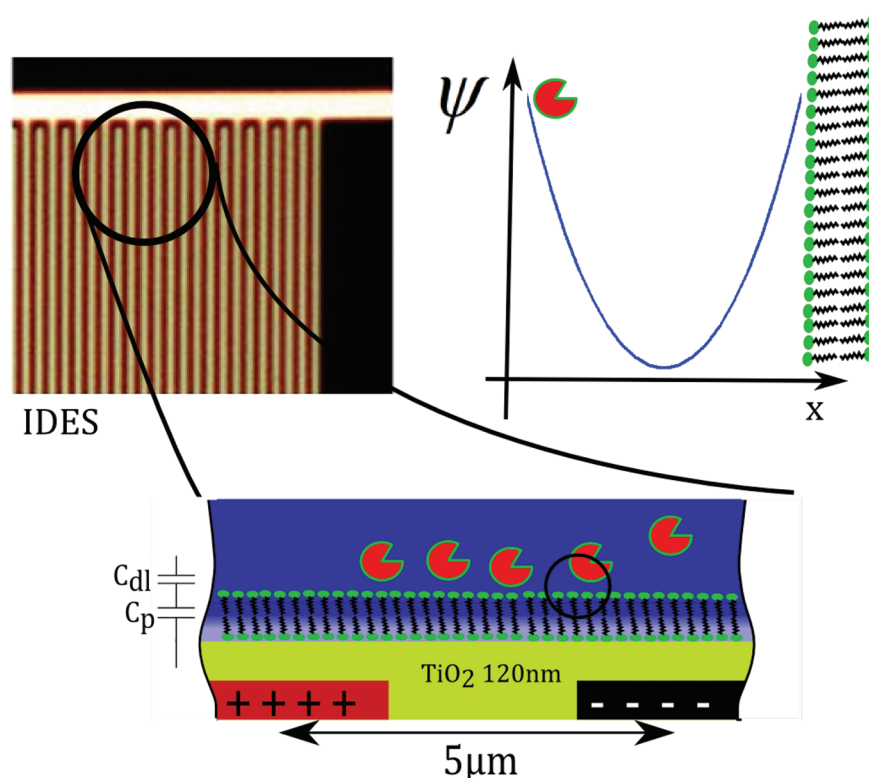
**Figure 1.** Picture of the $\mu$IDES and schematic representation of the experimental setup. Charged particles such as proteins approaching a lipid bilayer surface, induce a significant change in the potential distribution at the biointerface.

$$C_{dl} = \frac{d\sigma}{d\Psi} \qquad (7)$$

For simplicity, it will be referred to as the double layer capacitance. Solving the PB equation for an isolated surface leads to the Grahame equation for the surface charge[4]

$$\sigma = \sqrt{8c_0 \varepsilon \varepsilon_0 k_B T} \ \sinh\left(\frac{e\psi_0}{2k_B T}\right) \qquad (8)$$

$$
\begin{aligned}
C_{dl} &= \frac{d\sigma}{d\Psi} \\
&= \frac{d}{d\Psi} \sqrt{8c_0 \varepsilon \varepsilon_0 k_B T} \ \sinh\left(\frac{e\psi_0}{2k_B T}\right) \\
&= \varepsilon \varepsilon_0 \kappa \ \cosh\left(\frac{e\psi_0}{2k_B T}\right)
\end{aligned}
\qquad (9)
$$

Because $\cosh(x) \approx 1$ for small $x$ we can write

$$C_{dl,\text{isolated}} = \varepsilon \varepsilon_0 \kappa \qquad (10)$$

For the linearized double layer capacitance. Without loss of generality, the surface at $x = x_1$ is assumed to be fixed and the surface at $x = x_2$ is approaching it. Even if this distinction is arbitrary, it is convenient because the capacitance will be evaluated at the location of $x = x_1$, considered as the electrode in an experimental setting.

## ■ COMPUTATIONAL METHODS

Equation 1 was solved numerically by Multiphysics COMSOL v4.0 using CR boundary conditions. The 1D-poeq interface was used and the boundary conditions were set using the flux boundary condition from eq 5. The mash was refined on both boundaries to increase accuracy of the solution. The surfaces were set to 25 mV in the constant potential case or to the corresponding surface charge of an isolated surface. Also, in the case of a charge regulating boundary the potential was set to 25 mV in the case of an isolated surface. The other parameters were chosen to give a Debye length of 10 nm. The capacitance was then extracted using eq 6.

## ■ EXPERIMENTAL METHODS

**Biochip Design.** The biochip design and sensor configuration is shown in Figure 1, while fabrication and characterization of $\mu$IDES sensors are described in detail elsewhere.[18] The electrode structures were made using optical lithography by depositing a gold layer on a quartz glass substrate (Borofloat). The electrode finger spacing and width was 5 $\mu$m and the entire sensor consists of a total of 200 individual fingers with a length of 1.075 mm. This results in a total electrode area of 1 mm$^2$. The electrodes were covered by a sputtered film of 120 nm titanium dioxide (Oerlikon Leybold Univtex 450 C). Using a PDMS well ($V_{\text{total}} = 100\ \mu$L), the analyte solution was added and allowed to interact with the titanium dioxide surface. Impedance measurements obtained from the space between the electrode fingers were used to measure double layer capacitances in the absence and presence of charged particles.

*Contactless Impedance Spectroscopy.* Impedance was measured using an Agilent 4284A LCR Meter for Frequencies between 1 kHz and 1 MHz with an applied AC potential of ±50 mV. Impedance was fit in the complex admittance plane to a depressed semicircle with a center below the real axis. This is the model of a constant phase element (CPE) in series with a resistor. The CPE element is frequently employed when using impedance spectroscopy with a solid−liquid interface and is

linked to surface inhomogeneities on the electrode surface. The double layer capacitance was extracted by equation[20]

$$C_{dl} = (R^{-1})^{1-1/n} Q^{1/n} \tag{11}$$

where $R$ is the resistance of the electrolyte solution and $Q$ and $n$ are the parameters of the CPE element. In contrast to open (in contact) impedance measurements, in the current setup the gold electrodes ($\mu$IDES) are completely insulated by a 120 nm insulating titanium dioxide layer and measurements are performed in the absence of an external reference electrode (two electrode setup). Measured impedance phase angles and additional cyclic voltammetry (CV) measurements (data not shown) further confirmed complete electrical insulation at the employed potential range. This means that no charge transfer between the electrodes and the electrolyte takes place. The interface can therefore be described as the capacitances of the titanium dioxide layer and the double layer capacitance as two parallel plate capacitors in series as seen in Figure 1. The capacitance of the titanium oxide layer is further assumed to remain constant during experimentation. Hence by applying a potential of $\pm50$ mV at the gold electrodes, only double layer capacitance are measured around the potential of thermodynamic equilibrium on the titanium dioxide surface, or the supported lipid bilayer, respectively.

*Surface Modification of Silica Beads and Zeta Potential Measurement.* Silica beads with an average diameter of 3 $\mu$m were obtained from Kisker-Biotech (PSI-3.0 with plain surface) in a concentration of 50 mg/mL. The following solutions were prepared prior to modification: a 0.01 M NaOH solution, an APTES-modification solution of 2% (v/v) (3-Aminopropyl)-triethoxysilane (98% APTES from Alfa Aesar, A10668) in methanol with 0.15 M acetic acid and a 2.0 mM NaCl solution. For surface modification, beads were separated from the solution by centrifugation (4 min at 3000$g$) and incubated in a series of solutions for 1 min each: 0.01 M NaOH, methanol, APTES-modification solution, methanol (twice). A variety of different bead solutions were centrifuged and the supernatants discarded. Both APTS-modified and plain silica beads were washed three times in a 2.0 mM NaCl solution and diluted to a final bead concentration of 5 mg/mL. A hemocytometer was used to confirm bead concentrations in the final suspensions. Beads suspensions from both APTES-modified and plain silica with a pH 8 were prepared immediately prior to experimentation.

*Supported Lipid Bilayer and Protein Solution.* To form a SLB on the TiO$_2$ surface, DOPC/DOPS containing liposomes were brought into contact with the TiO$_2$ surface which led to the development of a SLB.[25] The biochips were washed in DI-Water and cleaned in O$_2$-plasma for 1 min (PELCO easyGlow) prior to experimentation. Aliquots of Annexin A5 in 10 mM HEPS buffer +2 mM Ca$^{2+}$ (courtesy of Professor Alain R. Brisson) were prepared as described.[26] BSA was obtained from Sigma-Aldrich and 0.1 g of BSA were diluted in 10 mL of 1xPBS and used without further purification.

## RESULTS

**Analytical Results.** *Linear Double Layer Capacitance.* For a symmetrical system with a charge of $\sigma_0 = \sigma_1$ at $x_{0,1}$ the solution of eq 3 is

$$\psi(x) = \frac{\sigma_0}{\varepsilon\varepsilon_r\kappa} \frac{\sinh(\kappa x)}{\cosh(\kappa L)} \tag{12}$$

The double layer capacitance is hence

$$C_{dl}(L) = \frac{d\sigma}{d\psi}\bigg|_{x=x_1} = \varepsilon\varepsilon_r\kappa \coth(\kappa L) = C_{dl,\text{isolated}} \coth(\kappa L) \tag{13}$$

Equally, the double layer capacitance of dissimilar surfaces $\sigma_0 = -\sigma_1$ can be found to be

$$C_{dl}(L) = C_{dl,\text{isolated}} \tanh(\kappa L) \tag{14}$$

These two results show that the double layer capacitance is a function of the distance between the two surfaces and also depends on the sign of the charges. For CC boundaries, the double layer capacitance will increase for equally charged surfaces upon approach and decrease for dissimilar surfaces. Similar results can be derived for the CP boundary; however, the behavior of the capacitance in the case of dissimilar and equally charged surfaces is reversed. This behavior is comparable to the double layer capacitance of the electrostatic forces due to double layer attraction or repulsion. In the case of surfaces with equal surface potential, the repulsive force can be approximated by $\Pi(L) \approx \psi_0^2 \exp(-L\kappa)$.[4] The similarity between those results promoted the search for a general expression between force and double layer capacitance. The relationship between force and double layer capacitance can be derived in the linear approximation by recalling the definition of the Gibbs free energy of the double layer

$$g = -2 \int_0^{\psi_0(L)} \sigma \, d\psi' = -2 \int_0^{\sigma_0(L)} \frac{1}{C_{dl}(L)} \sigma' \, d\sigma$$
$$= -\frac{1}{C_{dl}(L)} \sigma_0^2 \tag{15}$$

The integration is readily calculated by assuming that the potential, and hence also the capacitance, is linear with the charge (DH-approximation) and by substituting $d\psi'$ using eq 7. In the CC case $\sigma_0(L) = \sigma_0$ the force per unit area between the two surfaces is then

$$\Pi(x) = -\frac{dg}{dL} = -\frac{dC_{dl}}{dL} \frac{\sigma_0^2}{C_{dl}^2} \tag{16}$$

Next, the double layer capacitance is split into two parts: the capacitance of the isolated surface and the change due to the interaction.

$$C_{dl}(L) = C_{dl,\text{isolated}} + C_\Delta(L) \tag{17}$$

If the change in the double layer capacitance is assumed to be small, the resulting change in capacitance is directly related to the change in the double layer and the measured force.

$$\Pi(L) = -\frac{dC_\Delta}{dL} \frac{\sigma_0^2}{C_0^2}, \quad C_0 >> C_\Delta \tag{18}$$

The above equation shows that the change in the double layer capacitance is proportionally related to the electrostatic force and opens the possibility to compare impedance measurements with double layer interactions measured by force measurements. Similar results are found for CP where the sign is reversed in eq 18. Usually the CC and CR boundaries are lower and upper bounds for the measured force in the CR case.[23] Because of the relation found in eq 18 we conclude that the CC and CR results are also bounds for the change in the double layer capacitance in the linear approximation. The

relation between (linear) double layer capacitance and force result is particularly interesting because it suggest that, similar to electrostatic force, a relationship exists between the capacitance derived from the one-dimensional case and the integral capacitance between two bodies of arbitrary shape. One approach originally used by Derjaguin employs integration assuming that the curvature of the surfaces is small compared to the decay length. The total change in the double layer capacitance is then[4]

$$C_{\Delta,3D} = C_{dl,3d} + A\Gamma(t) \int_D^\infty C_\Delta(L) \frac{dA_s}{dx}\, dL \qquad (19)$$

where $D$ is the distance between the two surfaces in the $z$ direction, $A$ is the surface area of the electrodes, $\Gamma(t)$ is the concentration of particles on the surface in number/m$^2$, and $A_s$ is the cross section area of the surfaces. $C_\Delta$ can be either the linear approximation from the DH-theory or the numerical results obtained from COMSOL. Because of the derived dependence between the double layer change and electrostatic force, it is extrapolated that the approximation (eq 19) holds for similar cases as the original force formula. Here derivations are observed for, e.g., small particle sizes. The use of other approximations as SEI may be necessary.

**COMSOL Simulations.** The full PB equation was numerically solved using COMSOL FEMTo in order to evaluate the validity of the capacitance calculated by DH-approximation. The resulting capacitance for different potentials using the constant charge boundary condition is shown in Figure 2a. For both equally and dissimilar charged surfaces, the DH results concur with the full nonlinear case, confirming that the linear approximation is valid. Also, the potentials of different magnitude, which were not treated in the DH analysis, roughly follow the $\tanh(\kappa L)$ and $\coth(\kappa L)$ curves. However, for CP ($p_1 = 0$ and $p_2 = 0$) the nonlinear analysis methods reveal a more complex picture. As it can be seen in Figure 2b (for clarity only the potentials of the same magnitude are shown), the double layer capacitance increases upon approach for surfaces of equal charge as predicted by the linear theory. However, also in the dissimilar case, the capacitance rises as shown in Figure 3a. These results contradict findings obtained from the linear analysis, thus highlighting the limited applicability of analyzing double layer capacity in the dissimilar case. A comparable deviation from the linear theory is linked to the higher order terms of the interaction energy for dissimilar surface potentials.[5]

Next the double layer capacitance is investigated in the presence of charge regulating behavior. The dependence of the double layer capacitance upon the overlap of the two double layers on the charge regulation parameter is shown in Figure 2b and highlighted in more detail in Figure 3. It can be clearly seen that even without a change in the surface potential, the double layer capacitance constitutes a function of the regulation behavior. Figure 3b shows decreasing capacitance with increasing charge regulation parameter $p_2$. However, at a constant potential surface, the interaction results always in a positive change of the double layer capacitance.

## ■ EXPERIMENTAL RESULTS

**Zeta Potential Measurements.** The Zeta potential of the bare silica beads is approximately −30 mV (with a Gaussian distribution of $\sigma$ = 10 mV) at pH 8, whereas APTES modified silica beads exhibited a Zeta potential distributed of approximately +9 mV ($\sigma$ = 5 mV). The insulating 120 nm
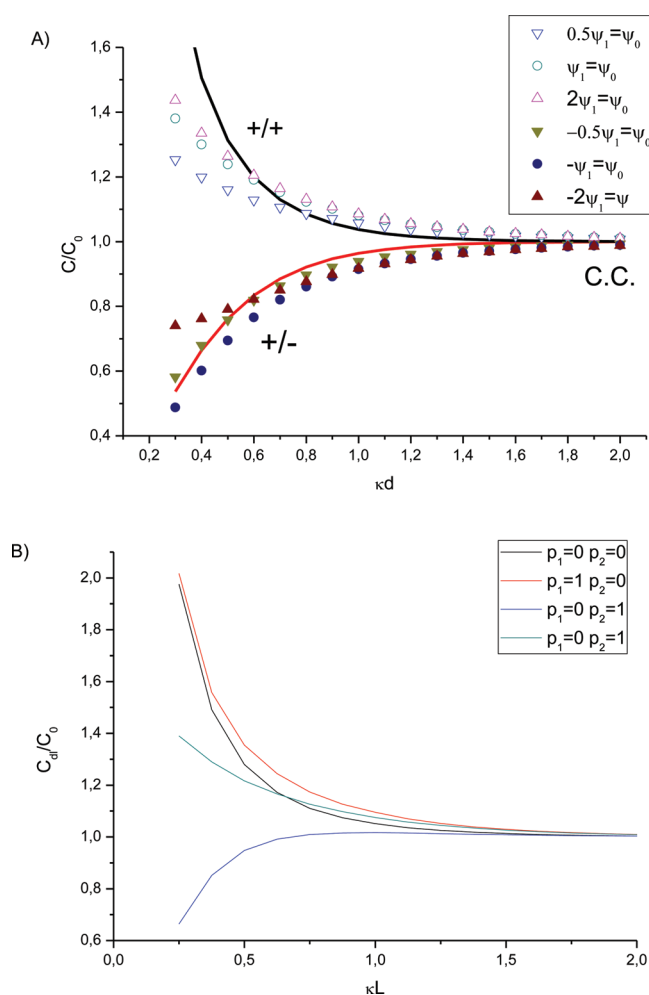


**Figure 2.** (A) Comparison between DH-approximation and PB equation. The capacitance is scaled to the value of infinitely separated plates. Solid lines show the results derived from eqs 5 and 6. Both equal and dissimilar CC boundary conditions ($p_1 = 1$ and $p_2 = 1$) are used. $\Psi_0 = 1$ in all graphs. (B) Double layer capacitance calculated for different values of the charge regulation parameter $p$ (both left and right boundary $p_1$ or $p_2$) and equally charged surfaces.

TiO$_2$ layer above the $\mu$IDES was found to be negatively charged featuring a Zeta potential of approximately −40 mV.

**Contactless Impedance Measurements.** The extracted double layer capacitance for increasing NaCl concentrations is shown in Figure 4. Since the capacitance of the TiO$_2$ surface is modeled in series with the double layer capacitance, the reciprocal capacitance is show as the $y$ axis. Consequently, the oxide capacitance appears in the constant $c$ of the LSQ Fit (see inset of Figure 4). The resulting root dependence of the double layer capacitance on the electrolyte concentration concords with the linear double layer capacitance from eq 10. It is important to note at this point that the commonly accepted impedance model consists of a capacitance (or CPE) and resistance in series where the double layer capacitance is assumed to be linear around the equilibrium potential of the surface.[27] In other words, the double layer capacitance is assumed to follow the DH-equation.

Impedance measurements in the presence of bare silica beads and APTES modified beads, as well as corresponding supernatant were conducted to investigate the influence of surface charges on double layer interaction. Figure 5a shows an
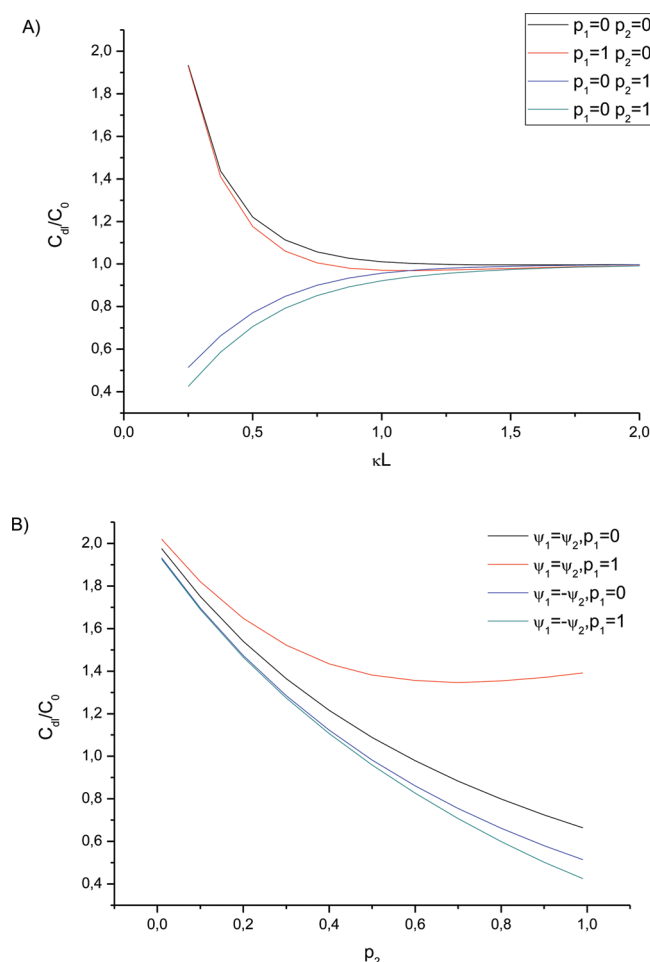
**Figure 3.** (A) Double layer capacitance obtained for different values of the charge regulation parameter $p$ (both left and right boundary $p_1$ or $p_2$) and dissimilarly charged surfaces. (B) Dependence of the double layer capacitance on the regulation behavior for a fixed distance of $\kappa L$ = 0.25. The capacitance is scaled to the capacitance of infinity separation showing that, depending on the regulation parameter $p_2$, both an increase and a decrease of the capacitance are displayed for the same surface charge.
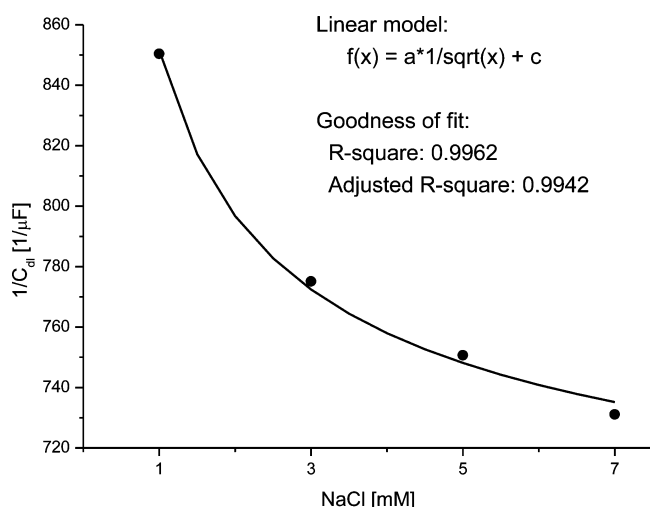


**Figure 4.** Reciprocal extracted double layer capacitance for increasing NaCl concentrations (full points). The straight line is a LSQ fit to $f(x)$.
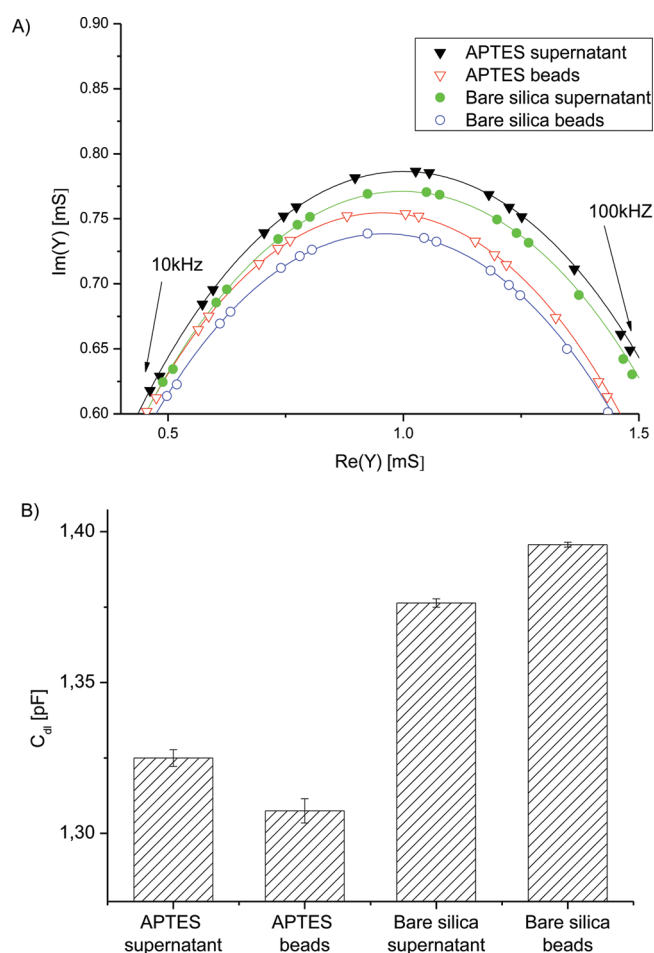


**Figure 5.** (A) Measured impedance (see inlet) and fit to the model (straight lines) and (B) the extracted double layer capacitance.

excellent agreement between the experimental data and the circuit model. The double layer capacitance was calculated using eq 11. In the case of bare silica beads, an increase in the double layer capacitance is seen, whereas in the case of the APTES modified beads, a decrease is observed.

The observed increases and decrease in capacitance can be directly attributed to the varying surface charges as determined by the Zeta potential measurements. The observed increase in the double layer capacitance in the presence of bare silica is of particular interest because a capacitance decrease could be expected due to limited current flow. In other words, because of their relatively large size, the beads (3 $\mu$m diameter) are expected to effectively decrease the surface area at the point of contact and to block the current flow due to the low dielectric constant of silica ($\varepsilon_r$ of approximately 6). The observed behavior can be explained (see red curve in Figure 5) by an increase of the double layer capacitance as described for a surface with $p_2 > 0.5$ (which was found by theoretical consideration in a 1-p$K$ model for silica surfaces)[6] and a regulation parameter near to 1 of $TiO_2$ (which is also common to metal oxides around the (pzc) point of zero charge set at approximately pH 6).[28] The above results clearly indicate that the diffuse double layer model is able to sufficiently describe the measured capacitance.

**Charge Regulation of Protein Adsorption Dynamics.** The adsorption of two different proteins on a supported lipid bilayer (SLB) that mimics a biointerface was investigated to

further highlight the importance of the charge regulation effect on the measured double layer capacitance. SLB and the proteins BSA and Annexin V are negativity charged at the applied pH (7.4).[26,29] In a first set of experiments, the nonspecific adsorption of BSA to the SLB was monitored and two distinctively different reaction kinetics can be seen in Figure 6a. The initial square root dependence is typical for a
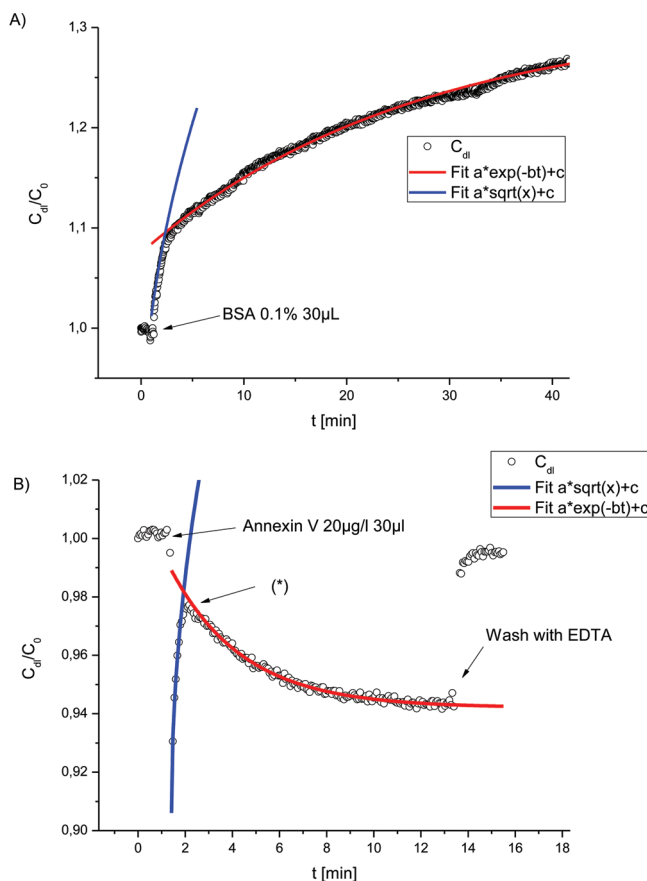


**Figure 6.** (A) Response of the double layer capacitance following the addition of 30 $\mu$L of 0.1% BSA. Two different kinetics can be identified with a square root dependence of $R^2 = 0.9753$ and a decaying exponential of $R^2 = 0.9959$. The fitting parameters are $a = 0.0021$ for the $\sqrt{x}$ fit, $a = -0.0916$, $b = 631.39$ $\mu$s, and $t_0 = 1.8534$ s for the $a \exp(-b(t - t_0))$ dependence and $c$ was found to be 0.8615 and 1.3222 respectively. (B) Response of the double layer capacitance following the addition of 30 $\mu$L of 20 $\mu$g/mL Annexin V. Two different kinetics can be identified, a square root dependence of $R^2 = 0.9912$ and a decaying exponential of $R^2 = 0.985$. The addition of the calcium ion complexing agent EDTA after 14 min induces immediate Annexin V desorption from the SBL, resulting in an impedance signal return to the baseline of the buffer solution. The fitting parameters are $a = 0.0136$ for the $\sqrt{x}$ fit, $a = 0.0055$, $b = 5.4$ ms, and $t_0 = 2.3054$ s for the $a \exp(-b(t - t_0))$ dependence and $c$ was found to be approximately 0.9411 for both fits.

mass-transport limited adsorption,[26] while the following exponential decay can be associated with a first order dynamics of a surface reaction limited process.[30] In turn, the surface charge density of BSA (see Figure 6a) was found to vary little at pH 7 pointing at a small inner or regulation capacitance.[29] This suggests a CP ($p_2 \rightarrow 0$) type dominated behavior of the system. As displayed in Figure 3b, a capacitance increase is expected to be independent of the exact charge regulating the behavior of the SLB. In a final set of experiments, the adsorption kinetics of

Annexin V to a SLB was studied. Annexin V belongs to a class of proteins that bind to a membrane by $Ca^{2+}$ induced conformational changes and the binding dynamics and calcium dependence has been intensively studied.[26] Figure 6b shows two different features that dominate the capacitance-time traces following the addition of Annexin V to a stable SLB background signal. Initially, as for the BSA case, a square root time dependence can be observed indicating that, in accordance with previous studies, Annexin V adsorption is mainly governed by mass-transport limited kinetics until confluence is reached.[26] The following secondary dynamics can again be described by an exponential function, as indicated with a (*) in Figure 6b. However the change in the double layer capacitance is now reversed.

A series of calculation were conducted to further determine whether the higher capacitance changes observed during Annexin V-SLB interaction compared to the changes observed during BSA-SLB adsorption can be linked to protein crystallization events. In previous studies it was shown that Annexin V is adsorbed in a distinct 2D-crystal structure on the membrane that can undergo a first order phase transition when it reaches a high surface concentration.[26,31] The above observed differences in adsorption dynamic between BSA and Annexin V further support the hypothesis that protein crystallization may have changed charge regulation behavior. To measure electrostatic interaction, and hence charge regulation, of proteins in situ based on contactless impedance spectroscopy could constitute an exciting new finding because it cannot be done with commonly used QCM-D instrumentation and AFM imaging.[26] The above results show that even though BSA and Annexin V are very different proteins in shape, potential and the type of interaction with the SLB the same qualitative dynamics can be identified. We therefore suggest that the observed capacitance change is not linearly connected to the absorbed amount on the surface as proposed in eq 19. The common underlining principle of the observed dynamic behavior is based on the electrostatic interaction of the proteins with the SLB surface and nearby proteins. The electrostatic interaction with nearby proteins changes the charge regulation properties, which can be understood by the results found by the regulation capacitance of the electrostatic interaction of two proteins:[24]

$$C_I = \langle Q^2 \rangle - \langle Q \rangle^2 \tag{20}$$

Here $\langle Q \rangle$ is the average overall orientation, ionizations states and position of the charge distribution of one isolated protein. From this relation it can be concluded that two proteins in close contact will have a different charge regulation capacitance due to the interaction of charges in close contact to each other, resulting in a new equilibrium charge distribution $Q$. We propose a model where the change in double layer capacitance consists of two different contributions $C_{\Delta,3D}^{p1}$ and $C_{\Delta,3D}^{p2}$ with concentrations $n_{1,2}(t)$.

$$C_{\Delta,3D} = n_1(t)C_{\Delta,3D}^{p1} + n_2(t)C_{\Delta,3D}^{p2}$$

$$\frac{dn_2(t)}{dt} = 2aD_2 n_1(t)$$

$$n_1(t) = \Gamma(t) - n_2(t) \tag{21}$$

Here $n_1(t)C_{\Delta,3D}^{p1}$ is the contribution of a isolated protein on the SLB. $n_2(t)C_{\Delta,3D}^{p2}$ describes the contribution of two proteins in electrostatic interaction. The concentration of $n_2(t)$ is

determined by assuming that the proteins are free to diffuse on the SLB, interact each time they collide and stay in close proximity.[32] Here $a$ is the radius of the particle and $D_2$ the diffusion constant of the protein on the SLB. The two capacitances relate to the two charge regulation parameters. In the presence of low surface concentration, a diffusion, or mass-transport, limited adsorption of the proteins to the surface with $\Gamma(t) = 2c(Dt/\pi)^{1/2}$ is assumed for Annexin V.[26] The fitted square root and decaying exponential observed in the experiment can be explained without solving the whole system. For the small $t$ the square root term will dominate and the double capacitance change follows the surface coverage. In turn, at higher protein concentrations the term $d\Gamma(t)/dt$ will go toward zero, resulting in a simple decaying exponential for the change in capacitance: $C_{\Delta,3D} \approx \exp(-t/\tau)$. The qualitative results of the two different scenarios are shown in Figure 7. In
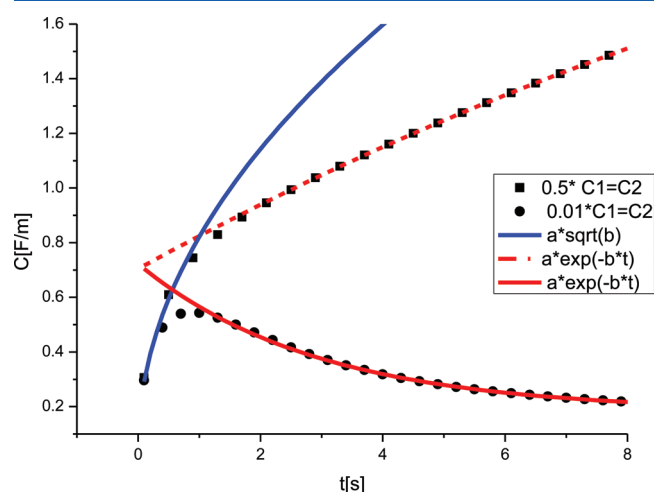


**Figure 7.** Solution of eq 21 for two sets of parameters (squares and dots). Except for the parameter $C_{\Delta,3D}{}^{p2}$ all other constants were set to unity.

the case of no or low particle interactions, the resulting behavior is comparable with BSA dynamics. Assuming that the charge regulation is changed significantly by the interaction of the proteins we find a dynamic similar to the Annexin V experiments. The square root dependence for small values of $t$ is not changed by this interaction as is expected. Although the same functions can be fitted for both scenarios, the full solution of eq 21 could not be fitted to the experimental data. This is probably due to the many parameters in eq 21 and needs to be studied further.

## CONCLUSION

In the current work contactless impedance spectroscopy was used to investigate double layer disruptions induced by charged particles at the biointerfaces $TiO_2$ and lipid-bilayers (SLB). Initially, changes to the double layer capacitance based on the overlap of two approaching charged surfaces were calculated using a linear approximation for both CC and CP boundary conditions. Analytical results obtained for surfaces exhibiting similar charges showed either a decrease or increase of the double layer capacitance depending on the applied boundary conditions and potentials. These results are in line with the effects of changing electrostatic force when a charged particle approaches. However, the linear approximation was found to be inadequate to describe the double layer capacitance in the

presence of dissimilar surface charges (even at low surface potentials of 25 mV). Consequently, a nonlinear capacitance was numerically computed and the effect of charge regulation on surface potential was included. Results of this study show that the measured capacitance is not only dependent on the surface potential, but it relies strongly on the charge regulation parameter. By employing contactless impedance spectroscopy, the interaction between positive and negatively charged silica beads with a titanium dixode surface was experimentally determined. The measured impedance signals are explained by a new model for the double layer capacitance that also includes a charge regulation (CR) parameter.

The newly developed model was then applied to assess charge shifts induced by double layer interactions at biologically relevant systems such as protein adsorption at a SLB. Results of BSA and Annexin V binding kinetics indicate that the adsorption dynamics can be monitored and coincide with previously reported QCM-D measurements. In addition to obtaining information on protein adsorption kinetics, we were also able to establish first indications of changed charge regulation behavior during protein surface crystallization events. Since charge regulation behavior cannot be detected using QCM-D, we intend to extend our existing study on protein assembly kinetics on supported lipid-bilayers.

## AUTHOR INFORMATION

**Corresponding Author**
*E-mail: peter.ertl@ait.ac.at. Fax: +43 (0) 50550 4399.

**Notes**
The authors declare no competing financial interest.

## REFERENCES

(1) Leckband, D.; Israelachvili, J. Q. Rev. Biophys. **2001**, 34 (2), 105−267.
(2) Marcelja, S. Biophys. J. **1992**, 61 (5), 1117−1121.
(3) Manciu, M.; Ruckenstein, E. Adv. Colloid Interface **2004**, 112 (1−3), 109−128.
(4) Butt, H.-J.; Graf, K.; Kappl, M. Physics and chemistry of interfaces; Wiley Verlag: Weinheim, Germany; 2003.
(5) Popa, I.; Sinha, P.; Finessi, M.; Maroni, P.; Papastavrou, G.; Borkovec, M. Phys. Rev. Lett. **2010**, 104 (22).
(6) Pericet-Camara, R.; Papastavrou, G.; Behrens, S. H.; Borkovec, M. J. Phys. Chem. B **2004**, 108 (50), 19467−19475.
(7) Behrens, S. H.; Borkovec, M. J. Phys. Chem. B **1999**, 103 (15), 2918−2928.
(8) Larson, I.; Drummond, C. J.; Chan, D. Y. C.; Grieser, F. J. Am. Chem. Soc. **1993**, 115 (25), 11885−11890.
(9) Butt, H. J. Biophys. J. **1991**, 60 (6), 1438−1444.
(10) Sokolov, I.; Ong, Q. K.; Shodiev, H.; Chechik, N.; James, D.; Oliver, M. J. Colloid Interface Sci. **2006**, 300 (2), 475−481.
(11) Camara, O. R.; Avalle, L. B.; Oliva, F. Y. Electrochim. Acta **2010**, 55 (15), 4519−4528.
(12) Evans, D.; Johnson, S.; Laurenson, S.; Davies, A. G.; Ko Ferrigno, P.; Walti, C. J. Biol. **2008**, 7 (1), 3.

(13) Rickert, J.; Gopel, W.; Beck, W.; Jung, G.; Heiduschka, P. *Biosens. Bioelectron.* **1996**, *11* (8), 757−768.

(14) Hartvig, R. A.; van de Weert, M.; Ostergaard, J.; Jorgensen, L.; Jensen, H. *Langmuir* **2012**, *28* (3), 1804−1815.

(15) Biesheuvel, P. M.; van der Veen, M.; Norde, W. *J. Phys. Chem. B* **2005**, *109* (9), 4172−4180.

(16) Hartvig, R. A.; v. d. W., M.; Østergaard, J.; Jorgensen, L.; Jensen, H. *Langmuir* **2011**, *27* (6), 2634−2643.

(17) Yardley, J. E.; Kell, D. B.; Barrett, J.; Davey, C. L. *Biotechnol. Genet. Eng. Rev.* **2000**, *17*, 3−35.

(18) Richter, L.; Charwat, V.; Jungreuthmayer, C.; Bellutti, F.; Brueckl, H.; Ertl, P. *Lab Chip* **2011**, *11* (15), 2551−2560.

(19) Gottschamel, J.; Richter, L.; Mak, A.; Jungreuthmayer, C.; Birnbaumer, G.; Milnera, M.; Brueckl, H.; Ertl, P. *Anal. Chem.* **2009**, *81* (20), 8503−8512.

(20) Brug, G. J.; Vandeneeden, A. L. G.; Sluytersrehbach, M.; Sluyters, J. H. *J. Electroanal. Chem.* **1984**, *176* (1−2), 275−295.

(21) Mirsky, V. M.; Riepl, M.; Wolfbeis, O. S. *Biosens. Bioelectron.* **1997**, *12* (9−10), 977−989.

(22) Das, P. K.; Bhattacharjee, S. *Langmuir* **2005**, *21* (10), 4755−4764.

(23) Carnie, S. L.; Chan, D. Y. C. *J. Colloid Interface Sci.* **1993**, *161* (1), 260−264.

(24) Lund, M.; Jonsson, B. *Biochemistry* **2005**, *44* (15), 5722−5727.

(25) Richter, R. P.; Berat, R.; Brisson, A. R. *Langmuir* **2006**, *22* (8), 3497−3505.

(26) Richter, R. P.; Him, J. L. K.; Tessier, B.; Tessier, C.; Brisson, A. R. *Biophys. J.* **2005**, *89* (5), 3372−3385.

(27) Daniels, J. S.; Anderson, E. P.; Lee, T. H.; Pourmand, N. *Conf. proc.: IEEE Eng. Med. Biol. Soc. Conf.* **2008**, *2008*, 5753−6.

(28) Kosmulski, M. *Adv. Colloid Interface* **2002**, *99* (3), 255−264.

(29) Salis, A.; Bostroem, M.; Medda, L.; Cugia, F.; Barse, B.; Parsons, D. F.; Ninham, B. W.; Monduzzi, M. *Langmuir* **2011**, *27* (18), 11597−11604.

(30) Edwards, P. R.; Lowe, P. A.; Leatherbarrow, R. J. *J. Mol. Recognit.* **1997**, *10* (3), 128−134.

(31) Reviakine, I.; Bergsma-Schutter, W.; Morozov, A. N.; Brisson, A. *Langmuir* **2001**, *17* (5), 1680−1686.

(32) Verwey, E. J. W.; Overbeek, J. Th. G *Theory of the Stability of Lyophobic Colloids*; Elsevier Publishing Company Inc.: Amsterdam, 1981.

**10469**

dx.doi.org/10.1021/jp3008392 | *J. Phys. Chem. B* 2012, 116, 10461−10469